Enhanced backscatter from one-dimensional random rough surfaces: stationary-phase approximations to full-wave solutions

E. Bahar and M. El-Shenawee

Department of Electrical Engineering/Center for Electro-Optics, University of Nebraska, Lincoln, Nebraska 68588-0511

Received August 13, 1993; revised manuscript received July 28, 1994; accepted August 3, 1994

We use the full-wave approach to obtain the solutions for the diffuse single- and double-scatter radar cross sections for one-dimensional rough surfaces. The solutions are expressed in terms of two- and six-dimensional integrals (not integral equations) for the single- and double-scatter cross sections. High-frequency, stationary-phase approximations are applied to these multidimensional expressions. The full-wave, high-frequency approximate solutions are obtained in closed forms for the single-scatter cross sections and in terms of two-dimensional integrals for the double-scatter cross sections. The sharp peak in the backscatter direction is due to the contributions from the double-scatter quasi-antiparallel paths. The level and the angular width of the enhanced backscatter peak are frequency dependent. The high-frequency approximations provide physical insight into the multiple-scatter problem. However, they cannot be used to predict accurately the angular width of the backscatter peak and the polarization dependence of the scatter cross sections.

1. INTRODUCTION

Integral expressions for the single and double incoherent diffuse scatter cross sections are obtained with the full-wave approach. These single- and double-scatter cross sections are expressed as two- and six-dimensional integrals, respectively. For rough surfaces with mean-square slopes $\langle h_x{}^2 \rangle \geq 0.5$ the double-scatter contribution to the total scatter cross section is significant even when the root-mean-square height is a fraction of the wavelength. Correlations between the heights and the slopes at pairs of points on the rough surface are accounted for in the analysis.

The CPU time needed to evaluate the six-dimensional integrals is excessive even for supercomputers. High-frequency, stationary-phase approximations are used here to reduce the six-dimensional integral expressions into two-dimensional integral expressions that are readily evaluated by computers. Using the high-frequency approximations, we also assume that the radii of curvature are large compared with the free-space wavelength. Thus the slope at two neighboring points (within a correlation length) is assumed to be equal to the slope at the midpoint.[1–5] The full-wave solutions are not restricted to Gaussian surface height and slope joint probability-density functions at two points on the surface, nor is it necessary to assume Gaussian surface height autocorrelation functions. The Fourier transform of the conditional joint characteristic function of the rough surface is shown to reduce to a Dirac delta function for the slopes at the specular points. Thus the slope-dependent surface element scattering coefficients are evaluated for slopes at the specular points.

The results show that the sharply enhanced backscatter is due to the contribution of the double-scatter quasi-antiparallel paths. The results based on the high-frequency approximations imply that there are no significant differences between the vertically and horizontally polarized scattered waves. The intensity fluctuations about the backscatter directions are also shown in the results. These fluctuations, which are observed in the experiments, are in part due to the interactions between two single-scatter intensities.

In this paper the rough surface is characterized by Gaussian joint probability-density functions for the surface heights and slopes at pairs of points on the surface. The surface height autocorrelation function and its Fourier transform (the rough-surface spectral density function) are also assumed to be Gaussian.

The derived scatter cross sections per unit footprint area are shown to be independent of the footprint area. It is shown here that the level and the angular width of the sharp peak in the enhanced backscatter direction are dependent on the frequency. The average (over the height) of the mean double-scatter path is introduced in the expressions of the double-scatter cross sections. It is shown that there is an optimum value for this parameter.

We use the high-frequency results to set up a tractable scheme to compute the full-wave six-dimensional integral expressions for the double-scatter cross sections as essentially three-dimensional integrals (a one-dimensional integral calls two, two-dimensional integrals[4]).

These results can be applied to the design and the fabrication of enhanced radar targets (inverse stealth) and road signs with broad angles of observation.

2. FORMULATION OF THE PROBLEM

For suppressed $\exp(j\omega t)$ time excitations the full-wave solutions for the diffuse double-scatter far fields $G_d^{fP}(\mathbf{r})$ from one-dimensional rough surfaces [$y = h(x)$] (Refs. 6–9) are

0740-3232/95/010151-11$06.00

$$R^V = \frac{\mu_r C_1^{in_1'} C_1^{fn_1'} \cos(\phi^{fn_1'} - \phi^{in_1'}) - S_0^{in_1'} S_0^{fn_1'}(1 - 1/\epsilon_r) + (1 - \mu_r)\cos(\phi^{fn_1'} - \phi^{in_1'})}{(C_0^{in_1'} + \eta_r C_0^{in_1'})(C_0^{fn_1'} + \eta_r C_1^{fn_1'})}, \quad (5b)$$

$$R^H = \frac{\epsilon_r C_1^{in_1'} C_1^{fn_1'} \cos(\phi^{fn_1'} - \phi^{in_1'}) - S_0^{in_1'} S_0^{fn_1'}(1 - 1/\mu_r) + (1 - \epsilon_r)\cos(\phi^{fn_1'} - \phi^{in_1'})}{(C_0^{in_1'} + C_1^{in_1'}/\eta_r)(C_0^{fn_1'} + C_1^{fn_1'}/\eta_r)}. \quad (5c)$$

$$G_d^{fP}(\mathbf{r}) = \frac{k_0^4}{4\pi^2} \frac{(2\pi)^{1/2}}{k_0 r} \exp(j\pi/4)\exp(-jk_0 r) \times \int \frac{D_{2'}(\hat{n}^f, \hat{n}')D_{1'}(\hat{n}', \hat{n}^i)}{[k_0(-n_y^i + n_y')][k_0(n_y^f - n_y')]} \times \exp[jk_0 x_{s2}'(n_x^f - n_x')] \times \exp[-jk_0 x_{s1}'(n_x^i - n_x')] \times \{\exp[-jk_0 h(x_{s1}')(n_y^i - n_y')] - 1\} \times \{\exp[jk_0 h(x_{s2}')(n_y^f - n_y')] - 1\} \times U(\mathbf{r}_{s1}')U(\mathbf{r}_{s2}') \frac{dn_y'}{(1 - n_y'^2)^{1/2}} dx_{s1}' dx_{s2}' G^{iP}(0), \quad P = V \text{ or } H, \quad (1)$$

where $\hat{n}^i$ and $\hat{n}^f$ are the unit vectors in the directions of the incident and scattered fields:

$$\hat{n}^i = n_x^i \hat{a}_x + n_y^i \hat{a}_y, \quad (2a)$$

$$\hat{n}^f = n_x^f \hat{a}_x + n_y^f \hat{a}_y, \quad (2b)$$

and the position vectors to points $1'$ and $2'$ on the rough surface are given by $\mathbf{r}_{s1}'$ and $\mathbf{r}_{s2}'$:

$$\mathbf{r}_{s1}' = x_{s1}'\hat{a}_x + h(x_{s1}')\hat{a}_y, \quad (3a)$$

$$\mathbf{r}_{s2}' = x_{s2}'\hat{a}_x + h(x_{s2}')\hat{a}_y. \quad (3b)$$

The wave vector in the direction of the fields scattered from the surface at $\mathbf{r}_{s1}'$ to the surface at $\mathbf{r}_{s2}'$ is (see Fig. 1)

$$\mathbf{k}_0' = k_0\hat{n}' = k_0(n_x'\hat{a}_x + n_y'\hat{a}_y), \quad (4)$$

where the free-space wave number is $k_0 = \omega(\mu_0\epsilon_0)^{1/2}$ and $\hat{n}'$ is a unit vector. The surface element scattering coefficients at points $\mathbf{r}_{s1}'$ and $\mathbf{r}_{s2}'$ on the surface are $D_{1'}(\hat{n}', \hat{n}^i)$ and $D_{2'}(\hat{n}^f, \hat{n}')$, respectively. The scattering coefficients depend on the polarizations of the incident and scattered waves, the media on both sides of the rough interface, and the local normals $\hat{n}_1'$ and $\hat{n}_2'$ at these points on the surface. The surface element scattering coefficients $D_{1'}(\hat{n}^f, \hat{n}')$ at point $1'$ on the surface are[6]

$$D_{1'}^P(\hat{n}^f, \hat{n}^i) = 2(\cos\theta_0^{fn_1'})(\cos\theta_0^{in_1'})R^P(\hat{n}^f, \hat{n}^i), \quad P = V \text{ or } H, \quad (5a)$$

where

In Eqs. (5) the dimensionless quantities η_r, ϵ_r, and μ_r are the relative intrinsic impedance, the relative permittivity, and the relative permeability, respectively, and $\hat{n}_1'$ is the unit vector normal to the rough surface at point $1'$. The angles of incidence and scatter in the local coordinate system are θ_0^{in} and θ_0^{fn}, respectively. Thus

$$C_0^{fn_1'} = \cos\theta_0^{fn_1'} = \hat{n}^f \cdot \hat{n}_1', \qquad C_0^{in_1'} = \cos\theta_0^{in_1'} = -\hat{n}^i \cdot \hat{n}_1', \quad (6)$$

and the corresponding sines of the incident and scatter angles are $S_0^{in_1'}$ and $S_0^{fn_1'}$. The angle between the local planes of incidence and scatter is given by[10]

$$\cos(\phi^{fn_1'} - \phi^{in_1'}) = \frac{(\hat{n}^f \times \hat{n}_1') \cdot (\hat{n}^i \times \hat{n}_1')}{|\hat{n}^f \times \hat{n}_1'|\,|\hat{n}^i \times \hat{n}_1'|}. \quad (7)$$

The angles $\theta_1^{in_1'}$ and $\theta_1^{fn_1'}$ for medium 1 beneath the interface are given by Snell's law:

$$S_1^{in_1'} = \sin\theta_1^{in_1'} = \sin\theta_0^{in_1'}/n_r,$$
$$S_1^{fn_1'} = \sin\theta_1^{fn_1'} = \sin\theta_0^{fn_1'}/n_r, \quad (8)$$

where $n_r = (\epsilon_r\mu_r)^{1/2}$ is the refractive index. Furthermore, $C_1^{in_1'}$ and $C_1^{fn_1'}$ are the corresponding cosines of the incident and scatter angles. The expressions for the surface element scattering coefficients $D_{2'}(\hat{n}^f, \hat{n}^i)$ at point $2'$ on the surface are similar to those for $D_{1'}(\hat{n}^f, \hat{n}^i)$.

In Eqs. (5) the superscripts denote the polarization of the incident and scatter waves, $P = V$ (vertical) or $P = H$ (horizontal). The vertically and horizontally polarized incident plane-wave amplitudes at the origin are $G^{iP}(0)$. For high frequencies the shadow function $U(\mathbf{r}_{s1})$ is equal to unity if the point at $\mathbf{r}_{s1}$ is illuminated by the incident waves $(\hat{n}^i)$ and visible at point $\mathbf{r}_{s2}'$; it is zero otherwise. Similarly, the shadow function $U(\mathbf{r}_{s2}')$ is equal to unity

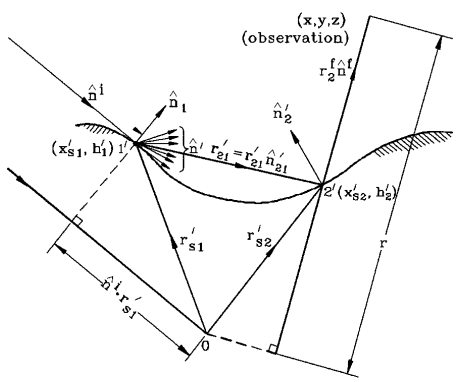

Fig. 1. Double-scatter electromagnetic waves.

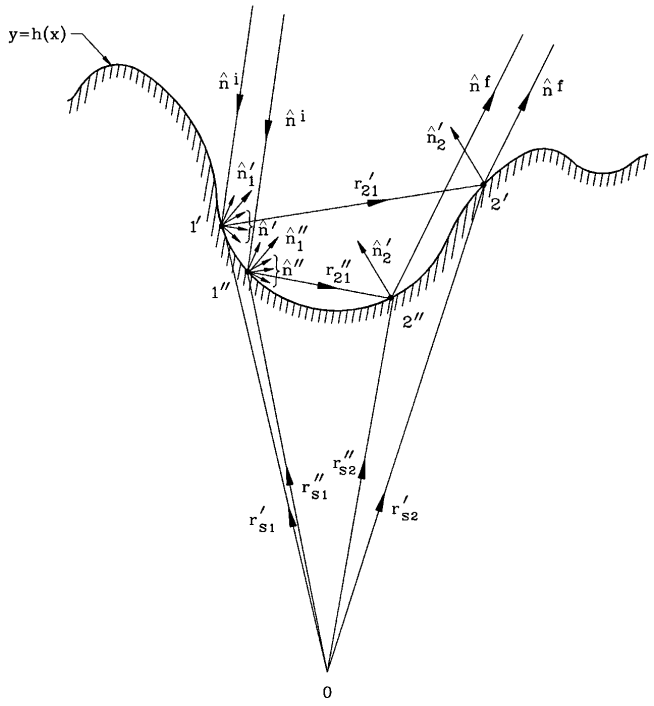

Fig. 2. Double-scatter intensity from one-dimensional random rough surfaces.

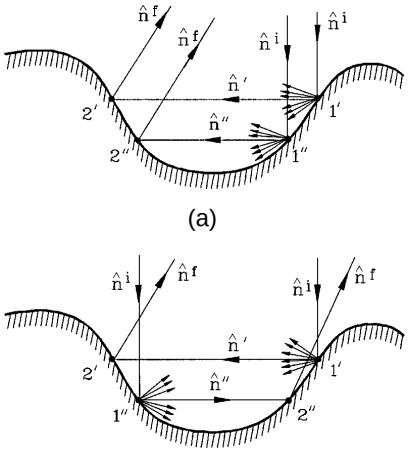

(a)

(b)

Fig. 3. (a) Quasi-parallel, regular path ($\hat{n}' \approx \hat{n}''$), (b) quasi-antiparallel, cross path ($\hat{n}' \approx -\hat{n}''$).

if the point at $\mathbf{r}'_{s2}$ is illuminated by a source at $\mathbf{r}'_{s1}$ and visible at the receiver ($\hat{n}^f$).[11] The distance to the receiver from the origin is given by $r = (x^2 + y^2)^{1/2}$.

The integrand for the diffuse double-scatter field expression given in Eq. (1) is not singular. The reason is that, as $k_0(n_y^i - n'_y) \to 0$ or as $k_0(n_y^f - n'_y) \to 0$, the numerator in the integrand of Eq. (1) is also proportional to $k_0(n_y^i - n'_y)$ and $k_0(n_y^f - n'_y)$ (see Appendix A). Also, as $n'_y \to \pm 1$, the fields scattered at $\mathbf{r}'_{s1}$ are parallel to the vertical y axis. For these double-scatter paths, $n'_y \to \pm 1$, the shadow functions $U(\mathbf{r}'_{s1}) = 0$ and $U(\mathbf{r}'_{s2}) = 0$, and the integrand vanishes.

We obtain the expression for the double-scatter field [Eq. (1)] on integrating by parts the iterative solution for the diffusely scattered field.[12] This expression does not contain the zero-order term.[13] The double-scatter intensity is obtained by multiplication of the expressions for the double-scatter fields [Eq. (1)] by their complex conjugate $[G_d^{fP}(\mathbf{r})]^*$ and integration over the height h and the slope h_x random variables. For convenience, $[G_d^{fP}(F)]^*$ is expressed in terms of different position vectors and wave-vector variables (denoted by double primes instead of single primes; see Fig. 2).

The incoherent quasi-parallel diffuse double-scatter cross section is therefore [see Fig. 3(a)]

$$\langle \sigma_{pdI} \rangle = \frac{{k_0}^7}{4\pi^2} (2L_m) P(\hat{n}^i) P(\hat{n}^f) \times \int_{n'_y=-\infty} \int_{n''_y=-\infty} \langle \sigma_{pdI1}(n'_y, n''_y) \rangle \langle \sigma_{pdI2}(n'_y, n''_y) \rangle \times [1 - P_2(|n'_y|)][1 - P_2(|n''_y|)] \mathrm{sinc}[k_0 L_m (n'_x - n''_x)] \times \frac{dn'_y}{[1 - (n'_y)^2]^{1/2}} \frac{dn''_y}{[1 - (n''_y)^2]^{1/2}}, \tag{9}$$

where $P_2(\hat{n})$ is the shadow function obtained by Sancer.[11,12]

In Eq. (9) the quasi-parallel double-scatter cross section is expressed in terms of a product of two terms $\langle \sigma_{pdIn} \rangle$ ($n = 1, 2$) associated with incoherent diffuse single-scatter cross sections:

$$\langle \sigma_{pdIn}(n'_y, n''_y) \rangle = \int_{x_{d1}=-2L}^{2L} \int_{h_{x1c}=-\infty}^{\infty} \frac{[D(\hat{n}', \hat{n}^i) D^*(\hat{n}'', \hat{n}^i)]_{h'_{xn}=h''_{xn}=h_{xnc}}}{[k_0(-n_y^i + n'_y)][k_0(-n_y^i + n''_y)]} \times [\chi_{2n}(a_n, b_n \mid h_{xnc}) - \chi_{2n}(a_n, 0 \mid h_{xnc}) - \chi_{2n}(0, b_n \mid h_{xnc}) - \chi(a_n)\chi(b_n) + \chi(a_n) + \chi(b_n)] \times \exp\left[jk_0 x_{dn} \left(-n_x^i + \frac{(n'_x + n''_x)}{2} \right) \right] p(h_{xnc}) \mathrm{d}h_{xnc} \mathrm{d}x_{dn}, \tag{10}$$

where x_{dn} and x_{cn}, the integration variables, are changed from x'_{s1}, x'_{s2}, x''_{s1}, and x''_{s2} to x_{d1}, x_{d2}, x_{c1}, and x_{c2}, with

$$x_{d1} = x'_{s1} - x''_{s1}, \qquad x_{d2} = x'_{s2} - x''_{s2}, \tag{11a}$$

$$x_{c1} = \frac{x'_{s1} + x''_{s1}}{2}, \qquad x_{c2} = \frac{x'_{s2} + x''_{s2}}{2}. \tag{11b}$$

In addition,

$$x_m = x_{c1} - x_{c2}, \qquad x_c = \frac{x_{c1} + x_{c2}}{2}, \tag{11c}$$

where the limits of integration for the variable x_c are $(-L, L)$. Furthermore, the limits of the integration with respect to x_m are $(-L_m, L_m)$, where L_m is the statistical average (over height) of the double-scatter mean path length.[12]

The conditional joint characteristic function for the heights h'_n and h''_n given the midpoint slope h_{xnc} is[12] (for $n = 1, 2$)

$$\chi_{2n}(a_n, b_n \mid h_{xnc}) = \exp\left[jh_{xnc} \frac{B_n}{\langle {h_x}^2 \rangle} (a_n - b_n) \right] \times \exp\left\{ \left[\langle h^2 \rangle (1 - R_n) - \frac{2{B_n}^2}{\langle {h_x}^2 \rangle} \right] a_n b_n \right\} \times \exp\left[-\frac{1}{2} \left(\langle h^2 \rangle - \frac{{B_n}^2}{\langle {h_x}^2 \rangle} \right) (a_n + b_n)^2 \right],$$

where

$$a_1 = k_0(-n_y^i + n_y'), \qquad b_1 = k_0(n_y^i - n_y''),$$
$$a_2 = k_0(n_y^f - n_y'), \qquad b_2 = k_0(-n_y^f + n_y''). \tag{12}$$

We obtain the coherent single-scatter cross sections $\langle\sigma_{pcn}\rangle$ on setting $R_n = 0$ in the expression for the total scatter field; thus, from Refs. 13 and 14,

$$\lim_{R_n\to 0} \chi_{2n}(a_n, b_n \,|\, h_{xnc}) = \chi(a_n)\chi(b_n), \tag{13a}$$

where

$$\chi(a_n) = \exp\left(-\frac{1}{2}\langle h^2\rangle a_n{}^2\right), \qquad \chi(b_n) = \exp\left(-\frac{1}{2}\langle h^2\rangle b_n{}^2\right). \tag{13b}$$

Furthermore,

$$\lim_{R_n\to 0} \chi_{2n}(a_n, 0 \,|\, h_{xnc}) = \chi(a_n), \tag{14a}$$
$$\lim_{R_n\to 0} \chi_{2n}(0, b_n \,|\, h_{xnc}) = \chi(b_n). \tag{14b}$$

The incoherent diffuse single-scatter cross sections are defined as

$$\langle\sigma_{pdIn}\rangle = \langle\sigma_{pdn}\rangle - \langle\sigma_{pcn}\rangle.$$

For the assumed Gaussian rough-surface spectral density function the normalized surface height autocorrelation functions are, for $n = 1, 2$,

$$R_n = \exp[-(x_{dn}/l_c)^2], \tag{15}$$

where l_c is the correlation length of the rough surface and

$$B_n = \langle h_n' h_{xnc}\rangle = \frac{\langle h^2\rangle}{l_c{}^2}\, x_{dn}\, \exp[-(x_{dn}/2l_c)^2] \tag{16a}$$
$$= \langle h_x{}^2\rangle \frac{x_{dn}}{2}\, \exp[-(x_{dn}/2l_c)^2]. \tag{16b}$$

Since the full-wave solutions account for upward and downward scattered waves, the quantities $-n_y^i + n_y'$, $-n_y^i + n_y''$, $-n_y^f + n_y'$, and $-n_y^f + n_y''$ could be positive or negative. The interaction between these two single-scatter cross sections is accounted for by the function $\mathrm{sinc}[k_0 L_m(n_x' - n_x'')]$. In Eq. (9) the integrand is equal to its complex conjugate when $\hat{n}'$ and $\hat{n}''$ are interchanged. The major contributions to the integrand in Eq. (9) come from the regions where $\hat{n}' \approx \hat{n}''$. In this region the arguments in the terms $\exp[-k_0{}^2\langle h^2\rangle(n_y' - n_y'')^2]$ and $\mathrm{sinc}[k_0 L_m(n_x' - n_x'')]$ are small. Thus Eq. (9) is referred to as the quasi-parallel ($\hat{n}' \approx \hat{n}''$) contribution to the double-scatter cross section.

At high frequencies the major contributions to Eq. (9) come from regions where x_{dn}/l_c is small. Thus the small x_{dn}/l_c expansion for the height/slope correlation B_n can be used:

$$\frac{B_n}{\langle h_x{}^2\rangle} = \frac{1}{2}\, x_{dn}\left[1 - \left(\frac{x_{dn}}{2l_c}\right)^2 + \frac{1}{2}\left(\frac{x_{dn}}{2l_c}\right)^4 - \ldots\right], \tag{17a}$$

$$\frac{B_n{}^2}{\langle h_x{}^2\rangle} = \frac{1}{2}\,\frac{\langle h^2\rangle}{l_c{}^2}\, x_{dn}{}^2\left[1 - 2(x_{dn}/2l_c)^2 + \frac{4(x_{dn}/2l_c)^4}{2!} - \ldots\right], \tag{17b}$$

$$1 - R_n = (x_{dn}/l_c)^2 - (x_{dn}/l_c)^4/2 + (x_{dn}/l_c)^6/6 - \ldots. \tag{17c}$$

Furthermore,

$$\langle h^2\rangle - \frac{B_n{}^2}{\langle h_x{}^2\rangle} = \langle h^2\rangle\left[1 - \frac{1}{2}(x_{dn}/l_c)^2 + (x_{dn}/l_c)^2(x_{dn}/2l_c)^2 - (x_{dn}/l_c)^2(x_{dn}/2l_c)^4 + \ldots\right], \tag{18a}$$

$$\langle h^2\rangle(1 - R_n) - \frac{2B_n{}^2}{\langle h_x{}^2\rangle} = \frac{\langle h^2\rangle}{24}\left(\frac{x_{dn}}{l_c}\right)^6 + O\left(\frac{x_{dn}}{l_c}\right)^8. \tag{18b}$$

On assuming that $a_n{}^2\langle h^2\rangle \gg 1$ and $b_n{}^2\langle h^2\rangle \gg 1$ (high-frequency approximations), we obtain $\chi(a_n) = \exp(-a_n{}^2\langle h^2\rangle/2) \ll 1$ and $\chi(b_n) = \exp(-b_n{}^2\langle h^2\rangle/2) \ll 1$. On keeping the leading terms in Eqs. (18) and substituting them into Eq. (10), one obtains

$$\langle\sigma_{pdI1}(n_y', n_y'')\rangle = \int_{x_{d1}=-2L}^{2L}\int_{h_{x1c}=-\infty}^{\infty} \frac{[D(\hat{n}', \hat{n}^i)D^*(\hat{n}'', \hat{n}^i)]_{h_{x1}'=h_{x1}''=h_{x1c}}}{[k_0(-n_y^i + n_y')][k_0(-n_y^i + n_y'')]} \times \exp\left\{jk_0 x_{d1}\left[\left(-n_x^i + \frac{n_x' + n_x''}{2}\right) + h_{x1c}\left(-n_y^i + \frac{n_y' + n_y''}{2}\right)\right]\right\} \times \exp\left[-\frac{1}{2}\, k_0{}^2\langle h^2\rangle(n_y' - n_y'')^2\right] p(h_{x1c})\mathrm{d}h_{x1c}\mathrm{d}x_{d1}. \tag{19a}$$

Similarly, from Eq. (10),

$$\langle\sigma_{pdI2}(n_y', n_y'')\rangle = \int_{x_{d2}=-2L}^{2L}\int_{h_{x2c}=-\infty}^{\infty} \frac{[D(\hat{n}^f, \hat{n}')D^*(\hat{n}^f, \hat{n}'')]_{h_{x2}''=h_{x2}''=h_{x2c}}}{[k_0(-n_y^f + n_y')][k_0(n_y^f + n_y'')]} \times \exp\left\{jk_0 x_{d2}\left[\left(n_x^f - \frac{n_x' + n_x''}{2}\right) + h_{x2c}\left(n_y^f - \frac{n_y' + n_y''}{2}\right)\right]\right\} \times \exp\left[-\frac{1}{2}\, k_0{}^2\langle h^2\rangle(n_y' - n_y'')^2\right] p(h_{x2c})\mathrm{d}h_{x2c}\mathrm{d}x_{d2}. \tag{19b}$$

Since the integrands in Eq. (10) vanish for large values of x_{dn} (compared with l_c), the limits of integration in Eqs. (19) with respect to the distance x_{dn} variables can be extended to infinity ($-\infty \le x_{dn} \le \infty$). Thus, integrating Eq. (19a) with respect to x_{d1}, one obtains

$$\langle\sigma_{pdI1}(n_y', n_y'')\rangle = \int_{h_{x1c}=-\infty}^{\infty} \frac{[D(\hat{n}', \hat{n}^i)D^*(\hat{n}'', \hat{n}^i)]_{h_{x1}'=h_{x1}''=h_{x1c}}}{[k_0(-n_y^i + n_y')][k_0(-n_y^i + n_y'')]} \left(\frac{2\pi}{k_0}\right) \times \delta\left[\left(-n_x^i + \frac{n_x' + n_x''}{2}\right) + h_{x1c}\left(-n_y^i + \frac{n_y' + n_y''}{2}\right)\right] \times \exp\left[-\frac{1}{2}\, k_0{}^2\langle h^2\rangle(n_y' - n_y'')^2\right] p(h_{x1c})\mathrm{d}h_{x1c}, \tag{20}$$

where the Dirac delta function is obtained from the Fourier transform of χ_2. On integrating Eq. (20) with respect to the slope h_{x1c}, one obtains the closed-form solution

$$\langle \sigma_{pdI1}(n_y', n_y'')\rangle = \left(\frac{2\pi}{k_0}\right)[D(\hat{n}', \hat{n}^i)D^*(\hat{n}'', \hat{n}^i)]_{h_{x1}'=h_{x1}''=h_{x1s}} \times \frac{p(h_{x1s})\exp[-\frac{1}{2}k_0^2\langle h^2\rangle(n_y' - n_y'')^2]}{[-n_y^i + (n_y' + n_y'')/2][k_0(-n_y^i + n_y')][k_0(-n_y^i + n_y'')]}, \tag{21a}$$

where

$$h_{x1s} = \frac{-[-n_x^i + (n_x' + n_x'')/2]}{-n_y^i + (n_y' + n_y'')/2}, \tag{21b}$$

in which h_{x1s} is the slope at the specular point where $\hat{n}_{1c} \rightarrow \hat{n}_{1s}$. Similarly, integrating Eq. (19b) with respect to the distance x_{d2} and the slope h_{x2c}, one obtains

$$\langle \sigma_{pdI2}(n_y', n_y'')\rangle = \left(\frac{2\pi}{k_0}\right)[D(\hat{n}^f, \hat{n}')D^*(\hat{n}^f, \hat{n}'')]_{h_{x2}'=h_{x2}''=h_{x2s}} \times \frac{p(h_{x2s})\exp[-\frac{1}{2}k_0^2\langle h^2\rangle(n_y' - n_y'')^2]}{[n_y^f - (n_y' + n_y'')/2][k_0(n_y^f - n_y')][k_0(n_y^f - n_y'')]}, \tag{22a}$$

where

$$h_{x2s} = \frac{-[-n_x^f + (n_x' + n_x'')/2]}{-n_x^f + (n_x' + n_x'')/2}, \tag{22b}$$

in which h_{x2s} is the slope at the specular point where $\hat{n}_{2c} \rightarrow \hat{n}_{2s}$. When we substitute Eqs. (21) and (22) into Eq. (9), the high-frequency quasi-parallel diffuse incoherent double-scatter cross section is obtained:

$$\begin{aligned}\langle \sigma_{pdI}\rangle = {} & k_0{}^5(2L_m)P(\hat{n}^i)P(\hat{n}^f) \\ & \times \int_{n_y'=-\infty}^{\infty}\int_{n_y''=-\infty}^{\infty}\left\{[D(\hat{n}', \hat{n}^i)D^*(\hat{n}'', \hat{n}^i)]_{h_{x1}'=h_{x1}''=h_{x1s}}\right. \\ & \left.\times \frac{p(h_{x1s})\exp[-\frac{1}{2}k_0^2\langle h^2\rangle(n_y' - n_y'')^2]}{[-n_y^i + (n_y' + n_y'')/2][k_0(-n_y^i + n_y')][k_0(-n_y^i + n_y'')]}\right\} \\ & \times \left\{[D(\hat{n}^f, \hat{n}')D^*(\hat{n}^f, \hat{n}'')]_{h_{x2}'=h_{x2}''=h_{x2s}}\right. \\ & \left.\times \frac{p(h_{x2s})\exp[-\frac{1}{2}k_0^2\langle h^2\rangle(n_y' - n_y'')^2]}{[n_y^f - (n_y' + n_y'')/2][k_0(n_y^f - n_y')][k_0(n_y^f + n_y'')]}\right\} \\ & \times [1 - P_2(|n_y'|)][1 - P_2(|n_y''|)]\mathrm{sinc}[k_0L_m(n_x' - n_x'')] \\ & \times \frac{\mathrm{d}n_y'}{[1 - (n_y')^2]^{1/2}}\,\frac{\mathrm{d}n_y''}{[1 - (n_y'')^2]^{1/2}}.\end{aligned} \tag{23}$$

In Eq. (23) the integrand is equal to its complex conjugate when $\hat{n}'$ and $\hat{n}''$ are interchanged. The major contributions to the integrand in Eq. (23) come from the regions where $\hat{n}' \approx \hat{n}''$ {where the arguments in the terms $\exp[-k_0{}^2\langle h^2\rangle(n_y' - n_y'')^2]$ and $\mathrm{sinc}[k_0L_m(n_x' - n_x'')]$ are small}.

For the quasi-antiparallel ($\hat{n}' \approx -\hat{n}''$) cross path [see Fig. 3(b)] the surface variables are grouped into the two pairs of points x_{s1}', x_{s2}'' and x_{s2}', x_{s1}''. In this case the following changes in the variables of integration are made instead of Eqs. (11):

$$x_{d1} = x_{s1}' - x_{s2}'', \qquad x_{d2} = x_{s2}' - x_{s1}'', \tag{24a}$$

$$x_{c1} = \frac{x_{s1}' + x_{s2}''}{2}, \qquad x_{c2} = \frac{x_{s2}' + x_{s1}''}{2}. \tag{24b}$$

It is also assumed for the quasi-antiparallel path that (consistent with the high-frequency assumption) the slopes at x_{s1}' and x_{s2}'' (h_{x1}' and h_{x2}'', respectively) on the rough surface are approximately equal to the slope h_{x1c} at the midpoint x_{c1} [see Fig. 3(b)]. Similarly, the slopes at the points x_{s2}' and x_{s1}'' (h_{x2}' and h_{x1}'', respectively) on the rough surface are equal to the slope h_{x2c} at the midpoint x_{c2} [see Fig. 3(b)]. The correlations between the heights at x_{s1}' and x_{s2}'' and the slope at x_{1c} are given by $\pm B_1$, and those between the heights at x_{s2}' and x_{s1}'' and the slope at x_{2c} are given by $\pm B_2$. The corresponding surface height autocorrelation functions at these pairs of points are given by R_1 and R_2. On substituting Eqs. (24) for the surface variables into the expression for the total diffuse scatter cross section (after performing all the algebraic manipulations similar to those for the quasi-parallel case), we obtain the expression for the incoherent diffuse double-scatter quasi-antiparallel cross section $\langle \sigma_{adI}\rangle$:

$$\begin{aligned}\langle \sigma_{adI}\rangle = {} & \frac{k_0{}^7}{4\pi^2}(2L_m)P(\hat{n}^i)P(\hat{n}^f) \\ & \times \int_{n_y'=-\infty}^{\infty}\int_{n_y''=-\infty}^{\infty}\langle \sigma_{adI1}(n_y', n_y'')\rangle\langle \sigma_{adI2}(n_y', n_y'')\rangle \\ & \times [1 - P_2(|n_y'|)][1 - P_2(|n_y''|)] \\ & \times \mathrm{sinc}[k_0L_m(n_x^f + n_x^i - n_x' - n_x'')] \\ & \times \frac{\mathrm{d}n_y'}{[1 - (n_y')^2]^{1/2}}\,\frac{\mathrm{d}n_y''}{[1 - (n_y'')^2]^{1/2}},\end{aligned} \tag{25}$$

in which $\langle \sigma_{adI1}(n_y', n_y'')\rangle$ is related to the single-scatter cross section given by

$$\begin{aligned}&\langle \sigma_{pdI1}(n_y', n_y'')\rangle \\ &= \int_{x_{d1}=-2L}^{2L}\int_{h_{x1c}=-\infty}^{\infty}\frac{[D(\hat{n}', \hat{n}^i)D^*(\hat{n}^f, \hat{n}'')]_{h_{x1}'=h_{x2}''=h_{x1c}}}{[k_0(n_y^i - n_y')][k_0(-n_y^f + n_y'')]} \\ &\quad \times [\chi_{21}(a_1, b_2\,|\,h_{x1c}) - \chi_{21}(a_1, 0\,|\,h_{x1c}) - \chi_{21}(0, b_2\,|\,h_{x1c}) \\ &\quad - \chi(a_1)\chi(b_2) + \chi(a_1) + \chi(b_2)] \\ &\quad \times \exp\left[jk_0\frac{x_{d1}}{2}(n_x^f - n_x^i + n_x' - n_x'')\right]p(h_{x1c})\mathrm{d}h_{x1c}\mathrm{d}x_{d1}\end{aligned} \tag{26a}$$

and $\langle \sigma_{adI2}(n_y', n_y'')\rangle$ is given by

$$\langle\sigma_{pdI2}(n_y', n_y'')\rangle = \int_{x_{d2}=-2L}^{2L}\int_{h_{x1c}=-\infty}^{\infty} \frac{[D(\hat{n}^f, \hat{n}')D^*(\hat{n}'', \hat{n}^i)]_{h_{x2}'=h_{x1}''=h_{x2c}}}{[k_0(n_y^f - n_y')][k_0(-n_y^i + n_y'')]} \times [\chi_{21}(a_2, b_1 \mid h_{x2c}) - \chi_{21}(a_2, 0 \mid h_{x2c}) - \chi_{21}(0, b_1 \mid h_{x2c}) - \chi(a_2)\chi(b_1) + \chi(a_2) + \chi(b_1)] \times \exp\left[jk_0 \frac{x_{d2}}{2}(n_x^f - n_x^i - n_x' + n_x'')\right] p(h_{x2c})\mathrm{d}h_{x2c}\mathrm{d}x_{d2}, \tag{26b}$$

where in this case (quasi-antiparallel) the conditional characteristic functions $\chi_{2n}(a_n, b_m \mid h_{xnc})$ $(n, m = 1, 2, m \neq n)$ and $\chi(a_n)$ and $\chi(b_n)$ are given by Eqs. (12) and (13b). The coherent single-scatter cross sections $\langle\sigma_{acn}\rangle$ can be obtained from Eqs. (13) if we set $R_n = 0$.

In Eq. (25) the diffuse double-scatter quasi-antiparallel cross section is expressed in terms of a product of two terms $\langle\sigma_{adn}\rangle$ $(n = 1, 2)$ associated with single-scatter cross sections. The interaction between these two single-scatter cross sections is accounted for by the function $\mathrm{sinc}[k_0L_m(n_x^f + n_x^i - n_x' - n_x'']$. The major contributions to the observed sharp backscatter enhancement come from the regions where the arguments of the terms $\exp[-k_0^2\langle h^2\rangle(-n_y^i + n_y'' - n_y^f + n_y')^2]$ and $\mathrm{sinc}[k_0L_m(n_x^f + n_x^i - n_x' - n_x'')]$ are very small and where $[1 - P_2(|n_y'|)][1 - P_2(|n_y''|)]$ is close to unity. This occurs for the antiparallel case $(\hat{n}' \approx -\hat{n}'')$ in the backscatter direction $(\hat{n}^f = -\hat{n}^i)$. The quasi-antiparallel double-scatter cross section accounts for the observed sharp backscatter enhancement.

When we apply the high-frequency approximations to the quasi-antiparallel diffuse incoherent double-scatter cross sections (25) (as we did in the quasi-parallel case), the terms associated with the single-scatter cross section are obtained in closed form:

$$\langle\sigma_{pdI1}(n_y', n_y'')\rangle = \left(\frac{2\pi}{k_0}\right)[D(\hat{n}', \hat{n}^i)D^*(\hat{n}^f, \hat{n}'')]_{h_{x1}'=h_{x2}''=h_{x1s}} \times \frac{p(h_{x1s})\exp[-\tfrac{1}{2}k_0\langle h^2\rangle(n_y^f + n_y^i - n_y'' - n_y')^2]}{(\tfrac{1}{2})(n_y^f - n_y^i - n_y' + n_y'')[k_0(n_y^i - n_y')][k_0(-n_y^f + n_y'')]}, \tag{27a}$$

where

$$h_{x1s} = \frac{-(n_x^f - n_x^i + n_x' - n_x'')}{n_y^f - n_y^i + n_y' - n_y''}, \tag{27b}$$

and

$$\langle\sigma_{pdI2}(n_y', n_y'')\rangle = \left(\frac{2\pi}{k_0}\right)[D(\hat{n}^f, \hat{n}')D^*(\hat{n}'', \hat{n}^i)]_{h_{x2}'=h_{x1}''=h_{x2s}} \times \frac{p(h_{x2s})\exp[-\tfrac{1}{2}k_0\langle h^2\rangle(n_y^f + n_y^i - n_y'' - n_y')^2]}{(\tfrac{1}{2})(n_y^f - n_y^i - n_y' + n_y'')[k_0(n_y^f - n_y')][k_0(-n_y^i + n_y'')]}, \tag{28a}$$

where

$$h_{x2s} = \frac{-(n_x^f - n_x^i - n_x' + n_x'')}{n_y^f - n_y^i - n_y' + n_y''}. \tag{28b}$$

On substituting Eqs. (27) and (28) into Eq. (25), we obtain the expression for the high-frequency double-scatter quasi-antiparallel cross section:

$$\langle\sigma_{adI}\rangle = \frac{{k_0}^7}{4\pi^2}(2L_m)P(\hat{n}^i)P(\hat{n}^f) \times \int_{n_y'=-\infty}^{\infty}\int_{n_y''=-\infty}^{\infty}\left\{\left(\frac{2\pi}{k_0}\right)[D(\hat{n}', \hat{n}^i)D^*(\hat{n}^f, \hat{n}'')]_{h_{x1}'=h_{x2}''=h_{x1s}} \times \frac{p(h_{x1s})\exp[-\tfrac{1}{2}{k_0}^2\langle h^2\rangle(n_y^f + n_y^i - n_y'' - n_y')^2]}{\tfrac{1}{2}(n_y^f - n_y^i + n_y' - n_y'')[k_0(n_y^i - n_y')][k_0(-n_y^f + n_y'')]}\right\} \times \left\{\left(\frac{2\pi}{k_0}\right)[D(\hat{n}^f, \hat{n}^i)D^*(\hat{n}'', \hat{n}^i)]_{h_{x2}'=h_{x1}''=h_{x2s}} \times \frac{p(h_{x2s})\exp[-\tfrac{1}{2}{k_0}^2\langle h^2\rangle(n_y^f + n_y^i - n_y'' - n_y')^2]}{\tfrac{1}{2}(n_y^f - n_y^i - n_y' + n_y'')[k_0(n_y^f - n_y')][k_0(-n_y^i + n_y'')]}\right\} \times [1 - P_2(|n_y'|)][1 - P_2(|n_y''|)] \times \mathrm{sinc}[k_0L_m(n_x^f + n_x^i - n_x' - n_x'')] \times \frac{\mathrm{d}n_y'}{[1 - (n_y')^2]^{1/2}}\frac{\mathrm{d}n_y''}{[1 - (n_y'')^2]^{1/2}}. \tag{29}$$

As in Eq. (23), the integrand in Eq. (29) is equal to its complex conjugate when $\hat{n}'$ and $\hat{n}''$ are interchanged. Thus, to evaluate Eqs. (23) and (29), it is necessary to evaluate only the real parts of the integrals within the limits $-1 \leq n_y' \leq 1$ and $-1 \leq n_y'' \leq n_y'$ or $n_y' \leq n_y'' \leq 1$ instead of evaluating both the real and the imaginary parts of the integral within the limits $-1 \leq n_y' \leq 1$ and $-1 \leq n_y'' \leq 1$. This speeds up the numerical evaluation of the integrals significantly and also increases the accuracy of the results.

For the quasi-parallel case the integrals in Eq. (23) must be evaluated for $n_x' = [1 - (n_y')^2]^{1/2}$, $n_x'' = [1 - (n_y'')^2]^{1/2}$ and for $n_x' = -[1 - (n_y')^2]^{1/2}$, $n_x'' = -[1 - (n_y'')^2]^{1/2}$. For the quasi-antiparallel case the integrals in Eq. (29) must be evaluated for $n_x' = [1 - (n_y')^2]^{1/2}$, $n_x'' = -[1 - (n_y'')^2]^{1/2}$ and for $n_x' = -[1 - (n_y')^2]^{1/2}$, $n_x'' = -[1 - (n_y'')^2]^{1/2}$.

Note that, using the high-frequency approximations (for the quasi-parallel and quasi-antiparallel cross sections) (23) and (29), we evaluate the slope-dependent surface element scattering coefficients D at the specular points on integrating with respect to the slopes h_{x1} and h_{x2}. Using the geometrical physical optics approach,[5] we evaluate the surface scattering coefficients *a priori* at the specular points.

With the use of Barrick's approach[5] it is shown that the same high-frequency approximations are obtained independent of the assumed Gaussian rough-surface statistics. The heights at the points at $\mathbf{r}_{s1}'$, $\mathbf{r}_{s1}''$, $\mathbf{r}_{s2}'$, and $\mathbf{r}_{s2}''$ on the rough surface are expanded about the height at the midpoints x_{c1} and x_{c2}. For the quasi-parallel case the heights h_1' and h_1'' are expanded about the height h_{c1} at the midpoint x_{c1}:

$$h_1' = h(x_{s1}') = h_{c1} + (x_{s1}' - x_{c1})\left.\frac{\partial h_1'}{\partial x}\right|_{x_{s1}'=x_{c1}}. \tag{30a}$$

$$h_1'' = h(x_{s1}'') = h_{c1} + (x_{s1}'' - x_{c1})\left.\frac{\partial h_1''}{\partial x}\right|_{x_{s1}''=x_{c1}}. \tag{30b}$$

Thus

$$h_1' - h_1'' = \left(\frac{x_{d1}}{2}\right)\left(\frac{\partial h_1'}{\partial x} + \frac{\partial h_1''}{\partial x}\right)\Bigg|_{x_{s1}'=x_{s1}''=x_{c1}} = x_{d1}h_{x1c}\,. \tag{30c}$$

Similarly, the heights h_2' and h_2'' are expanded about the height h_{c2} at the midpoint x_{c2}:

$$h_2' = h(x_{s2}') = h_{c2} + (x_{s2}' - x_{c2})\frac{\partial h_2'}{\partial x}\Bigg|_{x_{s2}'=x_{c2}}, \tag{31a}$$

$$h_2'' = h(x_{s2}'') = h_{c2} + (x_{s2}'' - x_{c2})\frac{\partial h_2''}{\partial x}\Bigg|_{x_{s2}''=x_{c2}}. \tag{31b}$$

Thus

$$h_2' - h_2'' = \left(\frac{x_{d2}}{2}\right)\left(\frac{\partial h_2'}{\partial x} + \frac{\partial h_2''}{\partial x}\right)\Bigg|_{x_{s2}'=x_{s2}''=x_{c2}} = x_{d2}h_{x2c}\,. \tag{31c}$$

The following approximations are also needed in this high-frequency analysis for the double-scatter cross sections:

$$h_2' - h_1' = h_{c2} - h_{c1} + \frac{x_{d2}}{2}h_{x2c} - \frac{x_{d1}}{2}h_{x1c}\,, \tag{32a}$$

$$h_2'' - h_1'' = h_{c2} - h_{c1} - \frac{x_{d2}}{2}h_{x2c} + \frac{x_{d1}}{2}h_{x1c}\,, \tag{32b}$$

where h_{x1c} and h_{x2c} are the slopes at the midpoints x_{c1} and x_{c2}. Thus the integrand is no longer dependent on the heights h_1', h_2', h_1'', and h_2''.

On integrating with respect to the distances x_{d1} and x_{d2}, one obtains the Dirac delta functions

$$\delta\left[\left(-n_x^i + \frac{n_x' + n_x''}{2}\right) + h_{x1c}\left(-n_y^i + \frac{n_y' + n_y''}{2}\right)\right],$$

$$\delta\left[\left(-n_x^f + \frac{n_x' + n_x''}{2}\right) + h_{x2c}\left(-n_y^f + \frac{n_y' + n_y''}{2}\right)\right].$$

Thus, on integrating over the slope variables h_{x1c} and h_{x2c}, one obtains the same solution [Eq. (23)] for the quasi-parallel cross section, even though the slope-dependent surface element scattering coefficients D were not *a priori* set equal to their values at the specular points. The geometrical/physical optics solution for the quasi-antiparallel cross section is also the same as the full-wave high-frequency solutions [Eq. (29)]. Note that, when Barrick's approach is used, the height/slope correlations and the surface height characteristics are not specified *a priori*.

The integration variables n_y' and n_y'' in Eqs. (23) and (29) are changed to θ' and θ'' through the substitutions $n_y' = \cos\theta'$ and $n_y'' = \cos\theta''$. Thus $n_x' = \pm[1 - (n_y')^2]^{1/2} = \pm\sin\theta'$ and $n_x'' = \pm[1 - (n_y'')^2]^{1/2} = \pm\sin\theta''$ for $-\pi \le \theta', \theta'' \le \pi$. The integrals are evaluated over only half the area, namely, $-\pi \le \theta' \le \pi$ and $-\pi \le \theta'' \le \theta'$ (or $\theta' \le \theta'' \le \pi$), since each half-integral is equal to the complex conjugate of the other half.

The corresponding high-frequency single-scatter cross-section solution is[10]

$$\langle\sigma\rangle = \frac{2\pi}{n_y^f - n_y^i}\,|D(\hat{n}^f, \hat{n}^i)|^2_{h_x=h_{xs2}}\,p(h_{xs})P_2(\hat{n}^f)P_2(\hat{n}^i)\,, \tag{33a}$$

where

$$h_{xs} = \frac{-(n_x^f - n_x^i)}{n_y^f - n_y^i}\,. \tag{33b}$$

We obtain the total cross section by incoherently adding the single- and double-scatter cross sections.

3. ILLUSTRATIVE EXAMPLES

The integrands of the two-dimensional integrals (23) and (29) are expressed as functions of the angles θ' and θ'' between the vertical y axis and the unit vectors $\hat{n}'$ and $\hat{n}''$, respectively. To illustrate the significance of the different contributions to the integrals (for both the quasi-parallel and the quasi-antiparallel paths), we have plotted the integrands as functions of θ' and θ'' (measured in radians) for $\theta^i = 10^\circ$ with $\phi^i - \phi^f = \pi$ and $\theta^f = 10^\circ$ backscatter in Fig. 4 and with $\theta^f = 5^\circ$ and $\phi^i - \phi^f = \pi$ in Fig. 5. The rough-surface mean-square height is given by the Rayleigh parameter $\beta = 4k_0^2\langle h^2\rangle = 41.077$, and the mean-square slope is $\langle h_x^2\rangle = 0.508$. Thus the correlation length is $l_c = 3.43\ \mu$m. The relative permittivity is $\epsilon_r = -424.64 - j81.144$ (gold), and the wavelength is $\lambda = 3.392\ \mu$m. The major contributions from the quasi-parallel path are along the diagonal $\theta' = \theta''$, and the major contributions from the quasi-antiparallel path are along the antidiagonal $\theta' = -\theta''$. The peaks are at $\theta' = \theta'' = \pm\pi/2$, since the shadow factor $[1 - P_2(|n_y'|)][1 - P_2(|n_y''|)] = 1$ when the scattered waves between points $1'$ and $2'$ ($1''$ and $2''$) are horizontal. Note that from Fig. 4 these contributions are equal (in the high-frequency limit) for only the backscatter case $\theta^i = \theta^f = 10^\circ$; however, for $\theta^i = 10^\circ$ and $\theta^i = 5^\circ$ ($\phi^i - \phi^f = \pi$) the contributions from the quasi-antiparallel path become relatively very small (see Fig. 5).

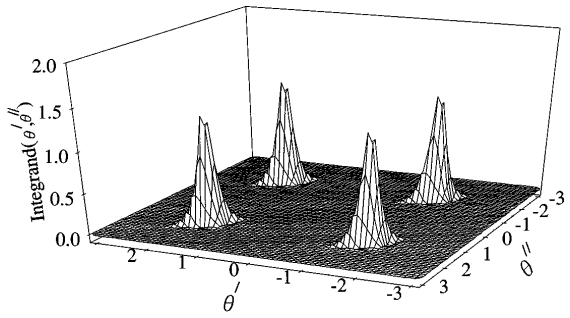

Fig. 4. Integrand of the double (quasi-parallel + quasi-antiparallel) scatter cross section plotted versus the angles θ' and θ'' for $\theta^i = 10^\circ$, $\theta^f = 10^\circ$, $\phi^i - \phi^f = \pi$, $\beta = 41.077$, $\langle h_x^2\rangle = 0.508$, $\lambda = 3.392\ \mu$m, and $\epsilon_r = -424.648 - j81.144$.

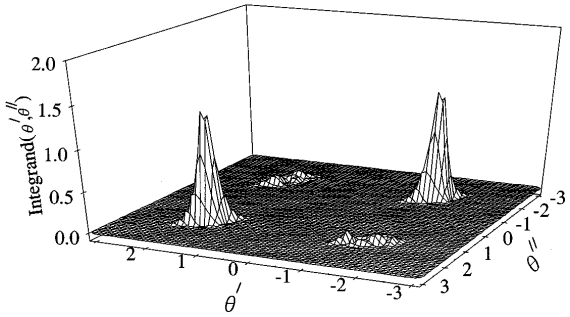

Fig. 5. Same as Fig. 4 but for $\theta^f = 5^\circ$.

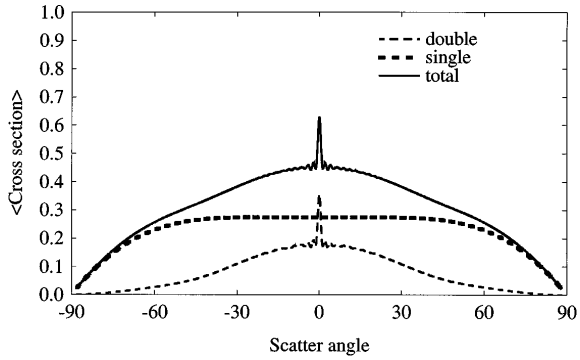

Fig. 6. Single, double, and total (single + double) scatter cross sections plotted versus the scatter angle (the scatter angle is defined as $\theta^f \cos \phi^f$ for $\phi^f = 0$, π and $\phi^i = 0$ for $\theta^i = 0$, $\beta = 356.128$, $\langle h_x{}^2 \rangle = 0.508$, $\lambda = 1.152\ \mu$m, and $\epsilon_r = -62.787 - j4.948$).

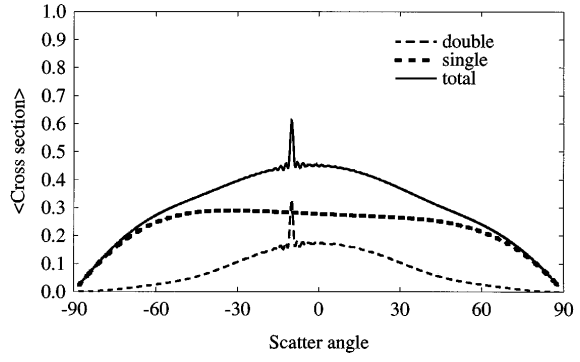

(a)

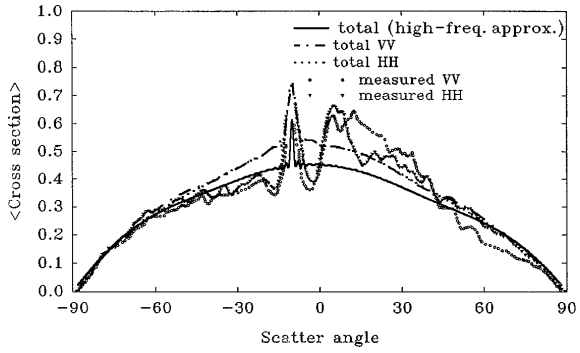

(b)

Fig. 7. (a) Same as Fig. 6 but for $\theta^i = 10^o$. (b) High-frequency results compared with solutions with the use of six-dimensional integrals[12] and measured data.[16] The parameters are the same as those in (a). VV, vertical polarization; HH, horizontal polarization.

In all the examples the double-scatter mean distance is assumed to be $L_m = 11.13 l_c$ (see Appendix B).[15]

The single- and double-scatter cross sections $\langle \sigma_I \rangle$ (quasi-parallel and quasi-antiparallel) are plotted in Figs. 6–11 as functions of $\theta^f \cos \phi^f$ (where $\phi^i - \phi^f = 0, \pi$) for the vertically and horizontally polarized waves. The incident angles are $\theta^i = 0^o$, 10°, and 30°. The one-dimensional rough surfaces considered in these examples are characterized by Gaussian surface height and slope probability-density functions. The root-mean-square height is $(\langle h^2 \rangle)^{1/2} = 1.73\ \mu$m, and the root-mean-square slope $\sqrt{h_x{}^2} = 0.712$ (the correlation length $l_c = 3.43\ \mu$m). Experimental data have been published recently for this surface.[16] The data presented here are renormalized such that the total power W scattered above the rough interface, per unit incident power, is

$$W = \int_0^{\pi/2} \langle \sigma_N \rangle_{\phi=0}\, \mathrm{d}\theta + \int_0^{\pi/2} \langle \sigma_N \rangle_{\phi=\pi}\, \mathrm{d}\theta\,.$$

Thus

$$\langle \sigma_N \rangle = \frac{\langle \sigma \rangle}{2\pi \cos \theta_0^i}\,.$$

In Figs. 6–8 the free-space wavelength is $\lambda = 1.152\ \mu$m, and in Figs. 9–11 the wavelength is $\lambda = 3.392\ \mu$m. The relative permittivity is $\epsilon_r = -62.787 - j4.948$ at $\lambda = 1.15\ \mu$m and $\epsilon_r = -424.64 - j81.144$ at $\lambda = 3.392\ \mu$m. The Rayleigh roughness parameter $\beta = 4k_0{}^2\langle h^2 \rangle = 356.128$ at $\lambda = 1.152\ \mu$m and $\beta = 41.077$ at $\lambda = 3.392\ \mu$m. The mean-square slope of the Gaussian rough surface is $\langle h_x{}^2 \rangle = 2\langle h^2 \rangle / l_c{}^2 = 0.508$.

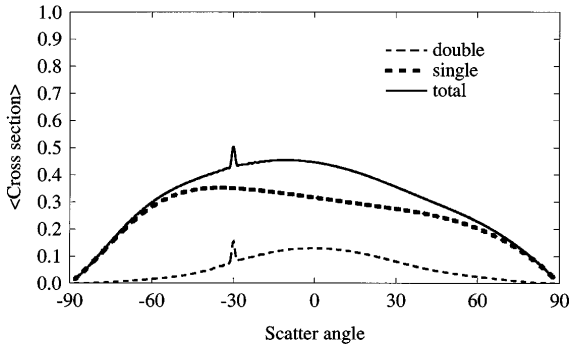

Fig. 8. Same as Fig. 6 but for $\theta^i = 30^o$.

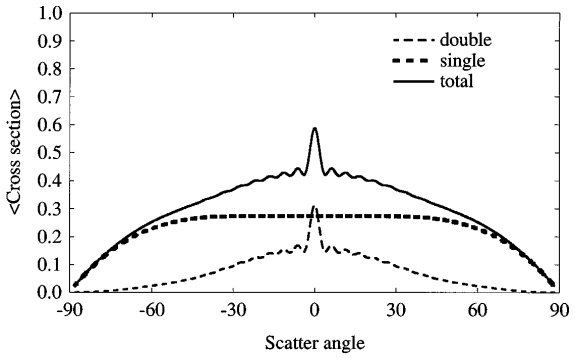

Fig. 9. Same as Fig. 6 but for $\theta^i = 0^o$, $\beta = 41.077$, $\langle h_x{}^2 \rangle = 0.508$, $\lambda = 3.392\ \mu$m, and $\epsilon_r = -424.648 - j81.144$.

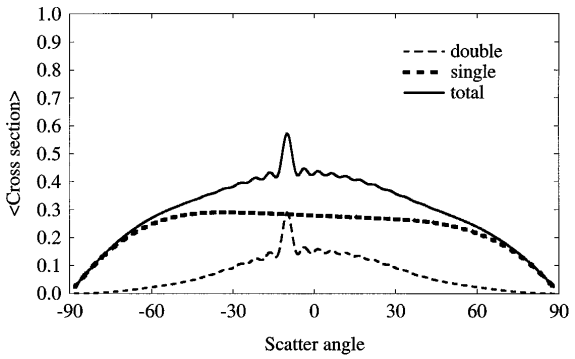

Fig. 10. Same as Fig. 9 but for $\theta^i = 10^o$.

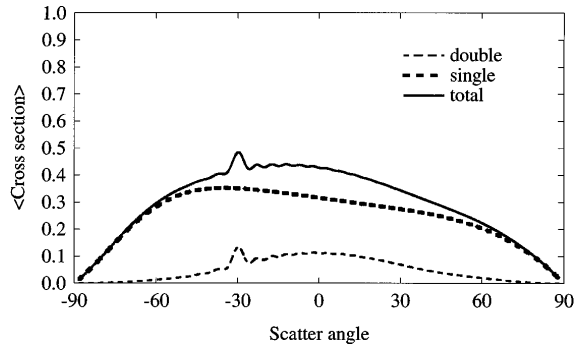

(a)

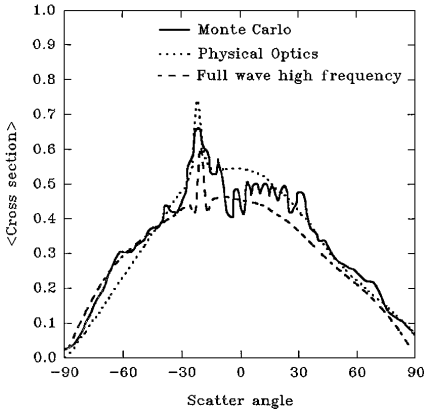

(b)

Fig. 11. (a) Same as Fig. 9 but for $\theta^i = 30^o$. (b) High-frequency results compared with those from physical optics[17] and Monte Carlo simulations.[16] The parameters are the same as those in (a), except that $\theta^i = 20^o$.

The sharp enhancement in the cross section $\langle\sigma\rangle$ for both the vertical and the horizontal polarizations occurs at backscatter, where $\theta^i = \theta^f$ and $\phi^i - \phi^f = \pi$. In Figs. 6 and 9 $\theta^i = 0^o$, in Figs. 7 and 10 $\theta^i = 10^o$, and in Figs. 8 and 11(a) $\theta^i = 30^o$. The enhanced backscatter is due to the contribution associated with the quasi-antiparallel path ($\hat{n}' = -\hat{n}''$) in the expression for the double-scatter cross sections [see Figs. 3(b), 4, and 5].

The high-frequency, full-wave results for the vertically and horizontally polarized scatter cross sections are practically indistinguishable. However, the full-wave results obtained from the six-dimensional integrals [Eqs. (9) and (25)] indicate that the double-scatter fields are polarization dependent.[4] At the stationary-phase points the surface element scattering coefficients [Eqs. (5)] are proportional to the Fresnel reflection coefficients.[10] For the highly reflective gold surface the magnitude of the Fresnel reflection coefficient is approximately equal to unity for both vertical and horizontal polarizations.

Comparing the results given in Figs. 6–8 with those given in Figs. 9–11 shows that the angular width of the sharp enhanced backscatter depends on frequency. The enhanced backscatter angular width is larger when $\lambda = 3.392$ μm (Figs. 9–11) than when $\lambda = 1.152$ μm (Figs. 6–8). When one compares the high-frequency results obtained in this paper and the high-frequency results obtained by Ishimaru *et al.*[17,18] with the full-wave results obtained from the six-dimensional integrals (9) and (25) (Ref. 4) and the experimental results,[16] it is clear that the angular width of the sharply enhanced backscatter and the polarization dependence have been significantly affected by the high-frequency approximations [see Figs. 7(b) and 11(b)]. Thus, even though the stationary-phase approximations used here are very useful in providing physical insight into the multiple-scatter problem, they cannot be used when the polarization dependence and the angular width of the enhanced backscatter peak are significant factors.

The high-frequency results derived here for the scatter cross sections per unit footprint area are independent of the footprint area. In this paper the evaluation of the mean double-scatter path L_m and its introduction into the expression for the double-scatter intensities are significantly different from the corresponding development by Ishimaru *et al.*[17,18] Ishimaru *et al.* introduced L_m through a Gaussian propagation tapering function. The intensity fluctuations about the backscatter directions are due to the interactions between the terms σ_{adI1} and σ_{adI2} associated with the single-scatter cross sections [Eqs. (26)] through the sinc function in Eq. (29). The argument of the sinc function is proportional to the mean double-scatter path L_m.

The mean-square height affects the level of the enhanced backscatter peak through the factor $\exp[-\frac{1}{2}k_0^2\langle h^2\rangle(n_y^i + n_y^f - n_y' - n_y'')]$ in the integrand of Eq. (29). Thus, as $k_0^2\langle h^2\rangle$ increases, the angular width of the enhanced backscatter peak decreases.

The mean-square slope also has a major effect on the level of the backscatter peak through the factor

$$\exp\left(\tfrac{1}{2}\langle h_x^2\rangle k_0^2\left\{\frac{x_{dn}}{2}\exp[-(x_{dn}/2l_c)^2]\right\}^2 \times (n_y^i + n_y^f - n_y' - n_y'')\right)$$

in the integrand of Eq. (29).

4. CONCLUSIONS

The high-frequency approximations were applied to the full-wave solutions for the single- and double-scatter cross sections. We incoherently added the single- and double-scatter cross sections to obtain the total cross section. The very sharp enhanced backscatter is due to the contribution of the double-scatter quasi-antiparallel path and not due to the single scatter.[19] We used the full-wave approach to obtain six- and two-dimensional integral expressions for the double- and single-scatter diffuse cross sections, respectively. Correlations between the heights and the slopes at pairs of points on the rough surface are accounted for in these expressions. The high-frequency, stationary-phase approximations are used in reduction of the expression for the double-scatter cross section from six- to two-dimensional integrals. We used the high-frequency results obtained from the two-dimensional integral expressions to set up a tractable scheme to evaluate the six-dimensional integrals (9) and (25).[4] The high-frequency approximations for the double scatter are practically independent of polarization, and the angular width of the enhanced backscatter is relatively small.

At high frequencies the major contributions to the double-scatter cross sections come from regions on the

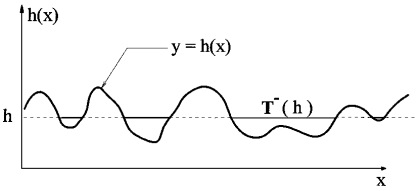

Fig. 12. Double-scatter mean path L_m [see Eqs. (B1) and (B2)].

surface where x_d/l_c are small. Thus, to obtain the high-frequency results, we expanded the correlation functions $B(x_d)$ and $A(x_d)$ (between the heights and the slopes at a pair of points on the surface) about x_d/l_c. On keeping the leading terms in these expansions, one obtains the high-frequency approximations to the full-wave solutions. As a result, the slope-dependent surface element scattering coefficients are evaluated at the specular points. Barrick's approach[5] is also indicated here. The same expressions for the high-frequency double-scatter cross sections [Eqs. (23) and (29)] are obtained independently of the assumed rough-surface height probability density function.

The full-wave expressions for the double-scatter cross sections [Eqs. (23) and (29)] contain expressions associated with two single-scatter cross sections. Using the high-frequency approximations, we evaluated these expressions [Eqs. (21), (22), (27), and (28)] in closed forms. The major contributions to the double-scatter integrals come from the regions where $\hat{n}' \approx \pm\hat{n}'' \approx \pm\hat{a}_x$ (near grazing angles with respect to the mean plane). The stationary-phase approximations used to evaluate the quantities [Eqs. (21), (22), (27), and (28)] are less valid at the grazing angles. Thus, while the high-frequency results are very useful in providing physical insight into the multiple-scatter problem, they do not provide satisfactory results for the polarization dependence and for the angular width of the enhanced backscatter.[4] The sinc function, which is a function of L_m (the mean double-scatter path), represents the interaction between the two single-scatter cross sections.

The effects of the shadowing P_2,[11] the mean double-scatter path L_m, the mean-square height $\langle h^2\rangle$, and the mean-square slope $\langle h_x{}^2\rangle$ on the double-scatter results are explicitly revealed in the analytical expressions for the full-wave quasi-parallel and quasi-antiparallel contributions to the cross sections. Thus the shadow function factors $[1 - P_2(|\hat{n}'|)][1 - P_2(|\hat{n}''|)]$ maximize the integrand when $\hat{n}'$ and $\hat{n}''$ are practically horizontal ($\hat{n}' \approx \pm\hat{n}'' \approx \pm\hat{a}_x$). The mean double-scatter path L_m (which appears in the sinc function) is responsible for the interaction between the terms that are associated with the single-scatter cross sections. The enhanced backscatter peak is maximum for $L_m \approx 25l_c$; however, the level of the backscatter peak is not critically dependent on L_m for $10l_c \le L_m \le 30l_c$ (see Appendix B).

APPENDIX A

If the mean plane of the rough surface is perpendicular to the unit vector $\hat{n}_0 = n_{0x}\hat{a}_x + n_{0y}\hat{a}_y$, the quantity [in the denominator of the integrand of Eq. (1)] $k_0(-n_y^i + n_y') = (-\hat{k}_0^i + \hat{k}_0') \cdot \hat{a}_y$ is replaced by $(-\hat{k}_0^i + \hat{k}_0') \cdot \hat{n}_0$ and the quantity $k_0(n_y^f - n_y') = (\hat{k}_0^f - \hat{k}_0') \cdot \hat{a}_y$ is replaced by $(\hat{k}_0^f - \hat{k}_0') \cdot \hat{n}_0$. Furthermore, $dx_{s1}' dx_{s2}'$ should be replaced by $[\mathrm{d}x_{s1}'/(\hat{n}_0 \cdot \hat{a}_y)][\mathrm{d}x_{s2}'/(\hat{n}_0 \cdot \hat{a}_y)]$.

In earlier research associated with single scatter[10] the quantities $(-\hat{k}_0^i + \hat{k}_0') \cdot \hat{n}_0$ and $(\hat{k}_0^f - \hat{k}_0') \cdot \hat{n}_0$ were used instead of $(-\hat{k}_0^i + \hat{k}_0') \cdot \hat{a}_y$ and $(\hat{k}_0^f - \hat{k}_0') \cdot \hat{a}_y$. However, for the small-slope case (the quantity in the denominator of the integrand) $(-\hat{k}_0^i + \hat{k}_0') \cdot \hat{n}(\hat{n} \cdot \hat{a}_y) \approx (-\hat{k}_0^i + \hat{k}_0') \cdot \hat{a}_y$ and $(\hat{k}_0^f - \hat{k}_0') \cdot \hat{n}(\hat{n} \cdot \hat{a}_y) \approx (\hat{k}_0^f - \hat{k}_0') \cdot \hat{a}_y$, and for the high-frequency case $(-\hat{k}_0^i + \hat{k}_0') \cdot \hat{n}_s(\hat{n}_s \cdot \hat{a}_y) \to (-\hat{k}_0^i + \hat{k}_0') \cdot \hat{a}_y$ and $(\hat{k}_0^f - \hat{k}_0') \cdot \hat{n}_s(\hat{n}_s \cdot \hat{a}_y) \to (\hat{k}_0^f - \hat{k}_0') \cdot \hat{a}_y$. Thus, in these limits, the earlier solutions give approximately the same results as those of the current solutions. However, when $(-\hat{k}_0^i + \hat{k}_0') \cdot \hat{a}_y \to 0$ or $(\hat{k}_0^f - \hat{k}_0') \cdot \hat{a}_y \to 0$, the two expressions could be significantly different.

The integrand of Eq. (1) remains finite as $(-\hat{k}_0^i + \hat{k}_0') \cdot \hat{a}_y = k_0(-n_y^i + n_y') \to 0$ or as $(\hat{k}_0^f - \hat{k}_0') \cdot \hat{a}_y = k_0(n_y^f - n_y') \to 0$, since in this case $\exp[-jk_0h(x_{s1}')(n_y^i - n_y')] - 1 \to -jk_0h(x_{s1}')(n_y^i - n_y')$ and $\exp[-jk_0h(x_{s2}')(n_y^f - n_y')] - 1 \to jk_0h(x_{s2}')(n_y^f - n_y')$.

APPENDIX B

We obtain the distance L_m by taking the statistical average of the mean distance $x_m = x_{c1} - x_{c2}$ [Eqs. (11c)] between the pairs of multiple-scatter points [see Figs. 3(a) and 3(b)]. In this paper the expression derived by Beckmann[15] for the mean duration of a fade $T^-(h)$ is used for the ensemble average of x_m. This ensemble average depends on the height h (level of signal[15]). Thus the average of this quantity over the heights is

$$L_m = \langle T^-(h)\rangle = \int_{h=-2\pi(\langle h^2\rangle)^{1/2}}^{h=2\pi(\langle h^2\rangle)^{1/2}} T^-(h)p(h)\mathrm{d}h\,, \tag{B1}$$

where the mean duration $T^-(h)$ is[15,18] (see Fig. 12)

$$T^-(h) = \frac{\pi}{\Omega}\exp(h^2/2\langle h^2\rangle)\left\{1 + \mathrm{erf}\left[\frac{h}{(2\langle h^2\rangle)^{1/2}}\right]\right\}. \tag{B2}$$

The probability-density function $p(h)$ of the height is assumed to be Gaussian truncated at $h = \pm 2\pi(\langle h^2\rangle)^{1/2}\{p[\pm 2\pi(\langle h^2\rangle)^{1/2}] = 1.067 \times 10^{-9}\}$. The constant $\Omega = \sqrt{2}/l_c$, where l_c is the correlation length. Since $\mathrm{erf}(x) = -\mathrm{erf}(-x)$, $L_m = 2\pi\sqrt{\pi}\,l_c = 11.13l_c$. The full-wave results are relatively insensitive to values of L_m between $10l_c$ and $30l_c$.

ACKNOWLEDGMENTS

The computational task was conducted at the Cornell National Supercomputer Facility, supported by the National Science Foundation. This research was partially supported by the U. S. Army Research Office and the Center for Electro-Optics of the University of Nebraska–Lincoln. The authors thank R. E. Collin for his constructive comments and suggestions. The manuscript was prepared by Janet Carlson.

E. Bahar's e-mail address is bahar@dragon.unl.edu; his telephone numbers are 402-472-1966 and 402-472-1968.

REFERENCES

1. E. Bahar and M. El-Shenawee, "Full wave multiple scattering from one dimensional random rough surfaces and high frequency stationary phase approximations," in *Proceedings of the IEEE Antennas and Propagation Society International Symposium*, Ann Arbor, Mich., June 1993 (Institute of Electrical and Electronics Engineers, New York, 1993), pp. 1316–1319.
2. E. Bahar and M. El-Shenawee, "Multiple scattering from one dimensional random rough surfaces—full wave solutions," presented at the Progress in Electromagnetics Research Symposium, Pasadena, Calif., July 1993.
3. E. Bahar and M. El-Shenawee, "High frequency approximations to multiple scatter that exhibit enhanced backscatter," presented at the 1993 International Geoscience and Remote Sensing Symposium (IGARSS '93), Tokyo, Japan, August 1993.
4. E. Bahar and M. El-Shenawee, "Numerical method to compute TE and TM multiple scatter from rough surfaces exhibiting backscatter enhancement," presented at the Computation of Electromagnetic Fields (COMPUMAG) symposium, Miami, Fla., October 1993.
5. E. D. Barrick, "Relationship between slope probability density function and the physical optics integral in rough surface scattering," Proc. IEEE **56,** 1728–1729 (1968).
6. M. El-Shenawee, "Full wave multiple scattering and depolarization of electromagnetic fields from rough surfaces," Ph.D. dissertation (University of Nebraska, Lincoln, Nebr., 1991).
7. E. Bahar and M. El-Shenawee, "Full wave multiple scattering from rough surfaces," in *Proceedings of the IEEE Antennas and Propagation Society International Symposium & URSI Radio Science Meeting*, Dallas, Texas, May 1990 (Institute of Electrical and Electronics Engineers, New York, 1990), pp. 1548–1551.
8. E. Bahar and M. El-Shenawee, "Use of supercomputers to evaluate singly and doubly scattered electromagnetic fields from rough surfaces," IEEE Trans. Magn. **27,** 4287–4290 (1991).
9. E. Bahar and M. El-Shenawee, "Multiple scattering from random distributions of individual rough surface scatterers," in *Proceedings of the IEEE Antennas and Propagation Society International Symposium & URSI Radio Science Meeting,* Chicago, Ill., July 1992 (Institute of Electrical and Electronics Engineers, New York, 1992), pp. 1708–1711.
10. E. Bahar, "Full-wave solutions for the depolarization of the scattered radiation fields by rough surfaces of arbitrary slope," IEEE Trans. Antennas Propag. **AP-29,** 443–454 (1981).
11. M. I. Sancer, "Shadow-corrected electromagnetics scattering from a randomly rough surface," IEEE Trans. Antennas Propag. **AP-17,** 577–585 (1969).
12. E. Bahar and M. El-Shenawee, "Vertically and horizontally polarized diffuse double scatter cross sections of one dimensional rough surfaces that exhibit enhanced backscatter full wave solutions," J. Opt. Soc. Am. A **11,** 2271–2285 (1994).
13. E. Bahar, "Full wave analysis for rough surface diffuse, incoherent radar cross sections with height-slope correlations included," IEEE Trans. Antennas Propag. **39,** 1293–1304 (1991).
14. E. Bahar and Bom Son Lee, "Full wave solutions for rough-surface bistatic radar cross sections: comparison with small perturbation, physical optics, numerical, and experimental results," Radio Sci. **29,** 407–429 (1994).
15. P. Beckmann, *Elements of Applied Probability Theory* (Harcourt, Brace & World, New York, 1968), p. 173.
16. M. E. Knotts, T. R. Michel, and K. A. O'Donnell, "Comparison of theory and experiment in light scattering from a randomly rough surface," J. Opt. Soc. Am. A **10,** 928–941 (1993).
17. A. Ishimaru and J. S. Chen, "Scattering from very rough surfaces based on the modified second order Kirchhoff approximation with angular and propagation shadowing," J. Acoust. Soc. Am. **88,** 1877–1883 (1990).
18. P. H. A. Ishimaru, J. S. Chen, P. Phu, and K. Yoshitomi, "Numerical, analytical, and experimental studies of scattering from very rough surfaces and backscattering enhancement," Waves Random Media **1,** S91–S107 (1991).
19. E. Bahar and M. A. Fitzwater, "Depolarization and backscatter enhancement in light scattering from random rough surfaces: comparison of full-wave theory with experiment," J. Opt. Soc. Am. A **6,** 20–43 (1989).